

Single Qudit Control in ^{87}Sr via Optical Nuclear Electric Resonance

Johannes K. Krondorfer,^{1,*} Matthias Diez,^{1,2} and Andreas W. Hauser^{1,†}

¹*Institute of Experimental Physics, Graz University of Technology, Petersgasse 16, 8010 Graz, Austria*

²*Institute of Physics, University of Graz, Universitätsplatz 5, 8010 Graz, Austria*

(Dated: July 1, 2025)

Optical nuclear electric resonance (ONER) was recently proposed as a fast and robust single-qubit gate mechanism in ^{87}Sr . Here, we demonstrate that ONER enables purely optical single-qudit control, addressing multiple hyperfine ground-state transitions within the ten-dimensional nuclear spin manifold. We show that ONER achieves high-fidelity spin manipulations, exceeding fidelities of 99.9%, while maintaining coherence even under realistic noise sources. These results establish ONER as a scalable and experimentally viable platform for high-dimensional quantum computing and quantum information processing.

Keywords: optical nuclear electric resonance, quantum computing, nuclear spin, qudit control, single qudit gate, neutral atoms

Quantum information processing relies on the precise control of quantum states, traditionally implemented using qubits, which encode information in two-level systems. However, qudits, which utilize multi-level quantum states, can offer significant advantages, including increased performance per computational unit [1–3] and reduced circuit complexity [4]. As a result, qudit-based quantum computation has gained increasing interest across various quantum platforms, including superconducting circuits [5, 6], trapped ions [3, 7], and neutral atoms [8–11].

Among the various physical implementations, nuclear spin states of alkaline earth atoms in atomic lattices are particularly promising for qubit and qudit control, due to their long-lived qudit states, the theoretically well-understood hyperfine structure [12], their naturally emerging multiple spin states and the ability to precisely control their interactions with external fields [13, 14]. These properties have led to experimental demonstrations of high-fidelity qubit gates [15–18], erasure conversion [19], and midcircuit operations [20–22].

While many works focus on the lowest lying nuclear spin states for qubit encoding, high spin nuclei offer the possibility for qudit encoding in multiple spin states. The ^{87}Sr system, featuring a nuclear spin of $I = 9/2$, has been a recent subject of theoretical studies [8, 10], where quantum control is suggested via magnetic radio fields acting on hyperfine levels in the electronic ground state which are Stark-shifted to enable individual addressability. Selectivity and achievable Rabi frequencies are thus limited by the achieved energy splitting and the capability to localize the radio frequency magnetic field. Recently, the experimental implementation of single qudit control was also achieved in ^{87}Sr via two-photon Raman transitions, addressing the lowest four spin states. [11]

While standard Raman methods have successfully been applied for qubit [23] and qudit control [11] in ^{87}Sr ,

the reported Rabi frequencies are in the order of 1 kHz, and additional light shifts are necessary to avoid undesired spin mixing. To enhance the achievable Rabi frequencies, we recently proposed optical nuclear electric resonance (ONER) as an alternative approach to nuclear spin manipulation. [24–26] ONER leverages the interaction between the nuclear quadrupole moment and an optically induced electric field gradient and hyperfine interaction, enabling high-resolution nuclear spin transitions via amplitude-modulated laser light. Specifically, ONER only requires a single amplitude-modulated laser beam to enable nuclear spin control, simplifying experimental implementation and enhancing localization and individual control compared to magnetic control mechanisms. While previous studies demonstrated ONER for qubit control in ^{87}Sr [26], achieving Rabi frequencies in the order of tens of kHz, its extension to qudit control remains, up to now, unexplored.

In this letter, we demonstrate how ONER can be used to achieve precise qudit control across multiple nuclear spin states of ^{87}Sr , achieving Rabi frequencies in the order of tens of kHz. We compute optimal magnetic field strengths and laser parameters to enable selective, high-fidelity spin transitions. We demonstrate that, in principle, all one-level transitions can be addressed via the ONER method. Furthermore, we assess the stability of ONER-based qudit gates under typical noise sources, showing that single spin flip fidelities exceeding 99.9% can be achieved at realistic laboratory conditions.

We concentrate on the $(5s^2) ^1S_0 \rightarrow (5s5p) ^3P_1$ transition in ^{87}Sr to achieve nuclear spin control in the ground state via the ONER method. We show that several one-level transitions of the ten-dimensional ground state manifold can be addressed by careful selection of the laser parameters. The principle of ONER for qudit control in ^{87}Sr is illustrated in Figure 1, where specific laser frequencies and amplitude modulations can drive different one-level transitions. In the case of single qubit manipulation, [26] ONER requires only moderate magnetic field strengths (≈ 200 Gauss), just so that a Paschen-Back-like regime is entered for the states of in-

* johannes.krondorfer@gmail.com

† andreas.w.hauser@gmail.com

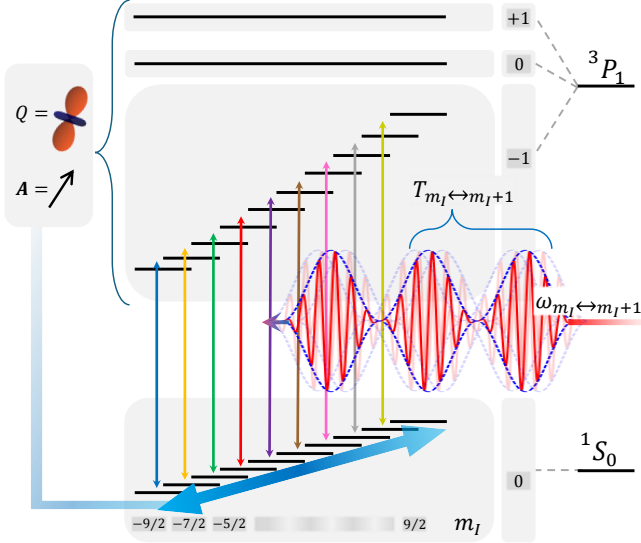


FIG. 1: Schematic illustration of the optical nuclear electric resonance (ONER) protocol applied to the level structure of the $(5s^2) ^1S_0 \rightarrow (5s5p) ^3P_1$ optical transition in ^{87}Sr for qudit control. Amplitude-modulated laser fields with periods $T_{m_I \leftrightarrow m_I+1}$, frequencies $\omega_{m_I \leftrightarrow m_I+1}$ and electronic Rabi frequency $\Omega_E/2\pi$ drive the system, resulting in an adiabatically modulated occupation of the electronically excited state. In the 1S_0 ground state, the magnetic nuclear spin quantum number m_I remains well-defined. In the 3P_1 excited states, the non-zero hyperfine interaction ($Q, A \neq 0$) mixes nuclear spin states. Which states are mixed can be selected via the laser frequency $\omega_{m_I \leftrightarrow m_I+1}$, which is chosen to be in between the respective spin levels in the $m_J = -1$ manifold. The amplitude modulation is adjusted to the specific transition, enabling several hyperfine nuclear spin transitions in the 1S_0 ground state.

terest in the hyperfine structure of the electronically excited state. However, for qudit control within the same protocol, higher magnetic fields will become necessary to access multiple spin states.

For a theoretical investigation, we consider the Hamiltonian of a ^{87}Sr atom in an external constant magnetic field \mathbf{B} in z -direction, and an amplitude-modulated laser field with modulation period T and polarization angle θ with respect to the z -axis within the rotating wave approximation (RWA). The amplitude modulation is set to $\Omega_E(t)/2\pi = \frac{\Omega_E/2\pi}{2} (1 - \cos(\frac{2\pi t}{T}))$. The total Hamiltonian is then given by

$$H = H'_E + H_Z + H_{\text{HF}} + H_{\text{AF}}(t), \quad (1)$$

with the electronic Hamiltonian in the rotating frame $H'_E = -\Delta |^3P_1\rangle\langle ^3P_1|$, with $\Delta = \omega_0 - \omega$, where ω_0 is the central transition frequency of the $(5s^2) ^1S_0 \rightarrow (5s5p) ^3P_1$ transition corresponding to 689 nm, and ω is the frequency of the laser field. Note that we set $\hbar = 1$ throughout the manuscript. The Zeeman Hamiltonian H_Z and

the hyperfine Hamiltonian H_{HF} are given by

$$H_Z = \left(g_J \mu_0 \hat{\mathbf{J}} - g_I \mu_N \hat{\mathbf{I}} \right) \cdot \mathbf{B}$$

$$H_{\text{HF}} = A \hat{\mathbf{I}} \cdot \hat{\mathbf{J}} + Q \frac{\frac{3}{2} \hat{\mathbf{I}} \cdot \hat{\mathbf{J}} (2\hat{\mathbf{I}} \cdot \hat{\mathbf{J}} + 1) - \hat{\mathbf{I}}^2 \hat{\mathbf{J}}^2}{2IJ(2I-1)(2J-1)}, \quad (2)$$

with the electronic total angular momentum $\hat{\mathbf{J}}$ and the nuclear spin $\hat{\mathbf{I}}$, both multiplied by their corresponding magneton (μ_0 and μ_N) and their g-factor, $g_J = 3/2$ and $g_I = -1.0928$, respectively.[27] The hyperfine constants are $A = 2\pi \times -260$ MHz and $Q = 2\pi \times -35$ MHz.[28] We choose a representation of the Hamiltonian in the basis $|n, m_J, m_I\rangle$, with n denoting the electronic state, and m_J, m_I denoting the magnetic quantum number of the total electronic angular momentum $\hat{\mathbf{J}}$ and nuclear spin $\hat{\mathbf{I}}$. In the dipole approximation, we then write the atom-field interaction Hamiltonian as

$$H_{\text{AF}}(t) = \frac{1}{2} \Omega_E(t) (\cos(\theta) |^1S_0\rangle \langle ^3P_1, 0| \otimes \mathbb{1} + \frac{\sin(\theta)}{\sqrt{2}} |^1S_0\rangle \langle ^3P_1, -1| \otimes \mathbb{1} - \frac{\sin(\theta)}{\sqrt{2}} |^1S_0\rangle \langle ^3P_1, +1| \otimes \mathbb{1} + c.c.), \quad (3)$$

with $\mathbb{1}$ denoting the unity matrix in the nuclear subspace. Additionally, we consider a decay from the 3P_1 state to the 1S_0 ground state with a decay rate of $\Gamma = 2\pi \times 7.48$ kHz.[23, 29]

We simulate the full time-dependent Hamiltonian given in Equation (1) within the Python library QuTiP[30, 31] using the Lindblad master equation[32] with decay Γ for the electronic levels. Via simulations of the full system, we identify parameters that lead to a spin flip between the m_I and $m_I + 1$ hyperfine ground states. For this purpose, we choose a laser frequency $\omega_{m_I \leftrightarrow m_I+1}$ exactly between the energies of the $|^1S_0, 0, m_I\rangle \rightarrow |^3P_1, -1, m_I\rangle$ and $|^1S_0, 0, m_I + 1\rangle \rightarrow |^3P_1, -1, m_I + 1\rangle$ transitions, i.e.

$$\omega_{m_I \leftrightarrow m_I+1} = \frac{1}{2} ((E(^3P_1, -1, m_I) - E(^1S_0, 0, m_I)) + (E(^3P_1, -1, m_I + 1) - E(^1S_0, 0, m_I + 1))), \quad (4)$$

as also illustrated in Figure 1. This choice enhances individual control of one-level nuclear spin transitions and reduces coupling to other $\Delta m_I = \pm 1$ transitions due to the detuning of the laser field from other transitions. Simultaneously, this choice of laser frequency ensures that m_I and $m_I + 1$ experience similar effective hyperfine interaction and show the same nuclear spin transition frequency. As illustrative example we choose a magnetic field of $B_0 = 3000$ G, a maximal electronic Rabi frequency $\Omega_{E,0}/2\pi = 30$ MHz, a polarization angle $\theta_0 = 60$ deg, and the laser frequency $\omega_{m_I \leftrightarrow m_I+1}$, respectively the detuning $\Delta_{m_I \leftrightarrow m_I+1}$, as specified in Equation (4). Extended scans for different parameters are provided in the Supplementary Information.

Scanning the amplitude modulation periods T , full flips of the nuclear spin typically appear for several equidistantly placed values of T .^[26] Their actual position depends on the magnetic field B_0 , the electronic Rabi frequency of the $^1S_0 \rightarrow ^3P_1$ transition $\Omega_{E,0}/2\pi$, and the angle θ_0 . This periodicity is caused by multi-photon-like transitions, where the amplitude modulation period matches an effective energy difference between the target spin states,

$$\Delta E_{m_I \leftrightarrow m_I+1}^{\text{eff}} = n \frac{2\pi}{T}, \quad (5)$$

for some $n \in \mathbb{N}$. Due to the time-dependent light shifts generated by the amplitude-modulated laser field, an analytical computation of the effective energy difference is unfeasible. While in principle multiple transition peaks occur, we investigate the first peak for the respective parameters, as the highest Rabi frequency and the smoothest transitions occur at this peak.

In Figure 2a we present nuclear spin-flip probabilities (colored lines),

$$P_{m_I \leftrightarrow m_I+1} = \max_{t \in \tau} |\langle ^1S_0, 0, m_I + 1 | \psi(t) \rangle|^2, \quad (6)$$

together with the resulting nuclear Rabi frequencies $\Omega_N/2\pi$ (colored crosses) at the transition peaks, as a function of the modulation period T . The probabilities are evaluated within a simulation interval $\tau = [0, 50 \mu\text{s}]$, where $|\psi(t)\rangle$ is the time-dependent wave function of the driven system, with $|\psi(0)\rangle = |^1S_0, 0, m_I\rangle$. Essentially, the flip probability $P_{m_I \leftrightarrow m_I+1}$ can be interpreted as the π -gate fidelity at the first flip for levels m_I and $m_I + 1$. Rabi oscillations at the maximum of the respective $m_I \leftrightarrow m_I + 1$ transition are illustrated in Figure 2b. For this parameter choice, all $\Delta m_I = \pm 1$ transitions can be independently addressed with high fidelity. Thus, ONER enables independent and high-fidelity control across the entire ^{87}Sr nuclear spin manifold, a critical requirement for practical qudit quantum operations. For lower magnetic fields, however, only transitions of low-energy hyperfine ground states can be addressed with high fidelity, as spin mixing will occur for transitions of higher states, since a sufficient Paschen-Back-like regime is not reached for those states. Nevertheless, one-level transitions between the ground and first excited hyperfine ground state can still be addressed with high fidelity. A more detailed analysis at different magnetic field strengths is provided in the Supplementary Information.

We now investigate the stability of the proposed ONER protocol for $m_I \rightarrow m_I + 1$ qudit transitions in the electronic ground state for the reference parameters given above. The stability is checked with respect to the laser parameters θ , Δ and Ω_E . Also, the robustness against variations in the magnetic field B and the amplitude modulation period T is tested. Concerning the role of heating and atom loss due to spontaneous scattering, we note that the simulation of the total system reveals that the occupation of the excited state is bounded by

$P_{3P_1} < 0.01$. The decay rate Γ for the 3P_1 state of ^{87}Sr leads to

$$N_{\text{sc}} = \frac{P_{3P_1} \Gamma}{\Omega_N} < 0.004 \quad (7)$$

as the total number of spontaneously scattered photons per Rabi cycle, assuming a nuclear Rabi frequency of $\Omega_N/2\pi \gtrsim 20$ kHz. Therefore, we can neglect heating and atom loss in this case.

To evaluate the stability with respect to the laser parameters and the magnetic field, we perform simulations with perturbed parameters and investigate the transition probability of the respective target states. We simulate the time evolution and calculate the π -pulse fidelity of the $|^1S_0, 0, m_I\rangle \leftrightarrow |^1S_0, 0, m_I + 1\rangle$ transition under perturbed parameters. The simulation results are summarized in Table I, where we show the minimum fidelity over all one-level transitions,

$$P_{\min} = \min_{m_I} P_{m_I \leftrightarrow m_I+1}. \quad (8)$$

Thus, if the deviation of each parameter is below the given threshold value for the target fidelity of 99% or 99.9%, all $\Delta m_I = \pm 1$ transitions can be addressed with the respective fidelity.

TABLE I: Tolerances for qudit control with ONER at $B_0 = 3000$ G, $\Omega_{E,0}/2\pi = 30$ MHz, $\theta_0 = 60$ deg, and the corresponding $\Delta_{m_I \leftrightarrow m_I+1}$ and $T_{m_I \leftrightarrow m_I+1}$. We show tolerances for the minimal flip probability P_{\min} , both for 99% and 99.9% target fidelities. Deviations smaller than the listed tolerances yield spin-flip control for all one-level transitions with the respective fidelity.

	$ \delta T $ (ns)	$ \delta B $ (mG)	$ \delta \Omega_E/2\pi $ (kHz)	$ \delta \theta $ (deg)	$ \delta \Delta $ (kHz)
99.9%	0.1	300	8	0.03	500
99%	0.6	3000	80	0.2	5000

Noise in the magnetic field up to 3 G ($\sim 0.1\%$ for $B_0 = 3000$ G) is tolerable for a π -pulse fidelity exceeding 99%. These tolerances are readily achieved with commercial power supplies, and are exceeded with modern stabilization techniques.^[33] Similar fidelities can be achieved with detunings from the optimal laser frequency of up to 5 MHz, a polarization angle perturbation of up to 0.2 degrees, and perturbations in the amplitude modulation period of up to 0.6 ns ($\sim 0.1\%$ for $T_{m_I,0} \approx 0.5 \mu\text{s}$). Noise in the electronic Rabi frequency Ω_E is tolerable up to 0.25%, equivalent to about 80 kHz. This translates into tolerable intensity noise of 0.5%, by using the relation $\Omega_E \sim \sqrt{I}$ and thus $\delta \Omega_E/\Omega_E = \frac{1}{2} \delta I/I$. Commercial stabilization systems readily achieve an intensity stability of 0.05%, which corresponds to 0.025% in electronic Rabi frequency. For small variations and fine-tuned control parameters, also fidelities exceeding 99.9% are possible.

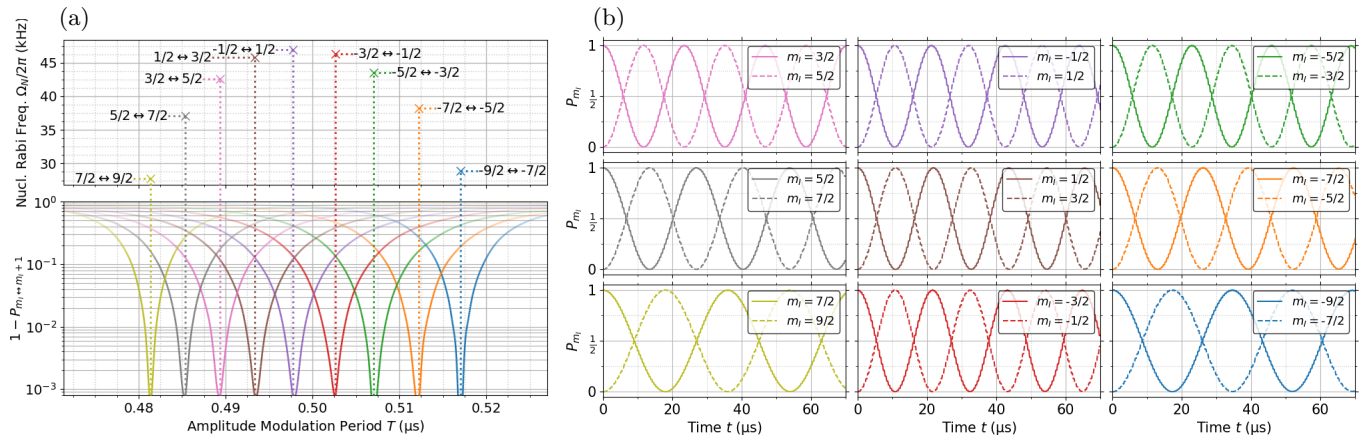


FIG. 2: (a) Amplitude modulation period scan and corresponding nuclear Rabi frequencies of $m_I \leftrightarrow m_I+1$ transitions. We show the π -pulse fidelity at the first flip $P_{m_I \leftrightarrow m_I+1}$ for all $\Delta m_I = \pm 1$ transitions at $B_0 = 3000$ G, $\Omega_{E,0}/2\pi = 30$ MHz, $\theta_0 = 60$ deg and $\Delta_{m_I \leftrightarrow m_I+1}$ as specified in Equation (4). Full transitions occur at different amplitude modulation periods $T_{m_I \leftrightarrow m_I+1}$ for different levels m_I . (b) Rabi oscillations of all $\Delta m_I = \pm 1$ at the optimal amplitude modulation period $T_{m_I \leftrightarrow m_I+1}$.

Thus, we observe stable results with respect to magnetic field perturbations, detuning, polarization angle, amplitude modulation period, and intensity, for experimentally reasonable parameter values and variations.

The stability analysis performed above shows the dependence of the tuning parameters and the stability with respect to quasi-static variations. The analysis remains valid as long as the timescale of the variations is large compared to the timescale of the gate operation. If this is not the case, the time-dependence of the variations has to be described with a suitable time-dependent noise model, fitted to the experimentally observable variations of the individual parameters.

In summary, we demonstrated that optical nuclear electric resonance (ONER) is a powerful method for rapid and robust single-qudit control in trapped neutral atoms. By selectively addressing multiple one-level nuclear spin transitions with tailored amplitude-modulated laser fields, we achieved fast qudit operations with high fidelity even in the presence of typical noise sources. This technique provides a compelling alternative to methods based on radio frequencies [8, 10] and standard two-photon Raman transitions [11, 23], by achieving higher nuclear Rabi frequencies and providing improved spatial localization, compared to magnetic control. While we focused our analysis on ^{87}Sr , which offers a total of 10 spin states, the method is equally applicable to

other alkaline earth and alkaline earth-like atoms. We demonstrated that ONER allows for qudit-gate operations at tens of kHz, surpassing the speed of conventional methods while maintaining coherence and scalability. Furthermore, high-fidelity operations could be achieved even in the presence of typical noise sources. This establishes ONER as a promising approach for scalable high-dimensional quantum computing, reducing circuit complexity and improving algorithmic efficiency. Given its robustness and experimental feasibility, the protocol opens new opportunities for qudit-based quantum error correction, high-dimensional entanglement, and quantum simulation. Future work will focus on lowering the required magnetic fields, extending ONER-based schemes to multi-qudit entanglement operations, and exploring their integration into large-scale neutral-atom quantum processors. Overall, ONER paves the way toward fast, coherent, and scalable high-dimensional quantum information processing.

We acknowledge funding by the Austrian Science Fund (FWF) [10.55776/P36903]. We further thank the IT Services (ZID) of the Graz University of Technology for providing high-performance computing resources and technical support.

-
- [1] E. T. Campbell, Enhanced fault-tolerant quantum computing in d -level systems, *Phys. Rev. Lett.* **113**, 230501 (2014).
 [2] Y. Chi, J. Huang, Z. Zhang, J. Mao, Z. Zhou, X. Chen, C. Zhai, J. Bao, T. Dai, H. Yuan, *et al.*, A programmable qudit-based quantum processor, *Nat. Commun.* **13**, 1166

- (2022).
 [3] M. Ringbauer, M. Meth, L. Postler, R. Stricker, R. Blatt, P. Schindler, and T. Monz, A universal qudit quantum processor with trapped ions, *Nat. Phys.*, 1053 (2022).
 [4] M. Luo and X. Wang, Universal quantum computation with qudits, *Sci. China Phys. Mech. Astron.* **57**, 1712

- (2014).
- [5] M. J. Peterer, S. J. Bader, X. Jin, F. Yan, A. Kamal, T. J. Gudmundsen, P. J. Leek, T. P. Orlando, W. D. Oliver, and S. Gustavsson, Coherence and decay of higher energy levels of a superconducting transmon qubit, *Phys. Rev. Lett.* **114**, 010501 (2015).
 - [6] E. Svetitsky, H. Suchowski, R. Resh, Y. Shalibo, N. Katz, Y. Rofer, H. Bluhm, D. Mahalu, and A. Frydman, Hidden two-qubit dynamics of a four-level josephson circuit, *Nature Communications* **5**, 5617 (2014).
 - [7] J. Randall, S. Weidt, E. D. Standing, K. Lake, S. C. Webster, D. F. Murgia, T. Navickas, K. Roth, and W. K. Hensinger, Efficient preparation and detection of microwave dressed-state qubits and qutrits with trapped ions, *Phys. Rev. A* **91**, 012322 (2015).
 - [8] S. Omanakuttan, A. Mitra, E. J. Meier, M. J. Martin, and I. H. Deutsch, Qudit entanglers using quantum optimal control, *PRX Quantum* **4**, 040333 (2023).
 - [9] T. V. Zache, D. González-Cuadra, and P. Zoller, Fermion-qudit quantum processors for simulating lattice gauge theories with matter, *Quantum* **7**, 1140 (2023).
 - [10] S. Omanakuttan, A. Mitra, M. J. Martin, and I. H. Deutsch, Quantum optimal control of ten-level nuclear spin qudits in ^{87}Sr , *Phys. Rev. A* **104**, L060401 (2021).
 - [11] H. Ahmed, A. Litvinov, P. Guesdon, E. Maréchal, J. H. Huckans, B. Pasquiou, B. Laburthe-Tolra, and M. R. de Saint-Vincent, Coherent control over the high-dimensional space of the nuclear spin of alkaline-earth atoms, arXiv preprint arXiv:2501.01731 10.48550/arXiv.2501.01731 (2025), arXiv:2501.01731 [quant-ph].
 - [12] M. M. Boyd, T. Zelevinsky, A. D. Ludlow, S. Blatt, T. Zanon-Willette, S. M. Foreman, and J. Ye, Nuclear spin effects in optical lattice clocks, *Phys. Rev. A* **76**, 022510 (2007).
 - [13] M. Saffman, Quantum computing with atomic qubits and rydberg interactions: progress and challenges, *J. Phys. B: At. Mol. Opt. Phys.* **49**, 202001 (2016).
 - [14] L. Henriët, L. Beguin, A. Signoles, T. Lahaye, A. Browaeys, G.-O. Reymond, and C. Jurczak, Quantum computing with neutral atoms, *Quantum* **4**, 327 (2020).
 - [15] A. Noguchi, Y. Eto, M. Ueda, and M. Kozuma, Quantum-state tomography of a single nuclear spin qubit of an optically manipulated ytterbium atom, *Phys. Rev. A* **84**, 030301 (2011).
 - [16] A. Jenkins, J. W. Lis, A. Senoo, W. F. McGrew, and A. M. Kaufman, Ytterbium nuclear-spin qubits in an optical tweezer array, *Phys. Rev. X* **12**, 021027 (2022).
 - [17] S. Ma, A. P. Burgers, G. Liu, J. Wilson, B. Zhang, and J. D. Thompson, Universal gate operations on nuclear spin qubits in an optical tweezer array of ^{171}Yb atoms, *Phys. Rev. X* **12**, 021028 (2022).
 - [18] J. A. Muniz, M. Stone, D. T. Stack, M. Jaffe, J. M. Kindem, L. Wadleigh, E. Zaly-Geller, X. Zhang, C. A. Chen, M. A. Norcia, J. Epstein, E. Halperin, F. Hummel, T. Wilkason, M. Li, K. Barnes, P. Battaglino, T. C. Bohdanowicz, G. Booth, A. Brown, M. O. Brown, W. B. Cairncross, K. Cassella, R. Coxe, D. Crow, M. Feldkamp, C. Griger, A. Heinz, A. M. W. Jones, H. Kim, J. King, K. Kotru, J. Lauigan, J. Marjanovic, E. Megidish, M. Meredith, M. McDonald, R. Morshead, S. Narayanaswami, C. Nishiguchi, T. Paule, K. A. Pawlak, K. L. Pudenz, D. R. Pérez, A. Ryou, J. Simon, A. Smull, M. Urbanek, R. J. M. van de Veerdonk, Z. Vendeiro, T. Y. Wu, X. Xie, and B. J. Bloom, High-fidelity universal gates in the ^{171}Yb ground state nuclear spin qubit, arXiv preprint arXiv:2411.11708 10.48550/arXiv.2411.11708 (2024), arXiv:2411.11708 [quant-ph].
 - [19] S. Ma, G. Liu, P. Peng, B. Zhang, S. Jandura, J. Claes, A. P. Burgers, G. Pupillo, S. Puri, and J. D. Thompson, High-fidelity gates and mid-circuit erasure conversion in an atomic qubit, *Nature* **622**, 279 (2023).
 - [20] J. W. Lis, A. Senoo, W. F. McGrew, F. Rönchen, A. Jenkins, and A. M. Kaufman, Midcircuit operations using the omg architecture in neutral atom arrays, *Phys. Rev. X* **13**, 041035 (2023).
 - [21] W. Huie, L. Li, N. Chen, X. Hu, Z. Jia, W. K. C. Sun, and J. P. Covey, Repetitive readout and real-time control of nuclear spin qubits in ^{171}Yb atoms, *PRX Quantum* **4**, 030337 (2023).
 - [22] M. A. Norcia, W. B. Cairncross, K. Barnes, P. Battaglino, A. Brown, M. O. Brown, K. Cassella, C.-A. Chen, R. Coxe, D. Crow, J. Epstein, C. Griger, A. M. W. Jones, H. Kim, J. M. Kindem, J. King, S. S. Kondov, K. Kotru, J. Lauigan, M. Li, M. Lu, E. Megidish, J. Marjanovic, M. McDonald, T. Mittiga, J. A. Muniz, S. Narayanaswami, C. Nishiguchi, R. Notermans, T. Paule, K. A. Pawlak, L. S. Peng, A. Ryou, A. Smull, D. Stack, M. Stone, A. Sucich, M. Urbanek, R. J. M. van de Veerdonk, Z. Vendeiro, T. Wilkason, T.-Y. Wu, X. Xie, X. Zhang, and B. J. Bloom, Midcircuit qubit measurement and rearrangement in a ^{171}Yb atomic array, *Phys. Rev. X* **13**, 041034 (2023).
 - [23] K. Barnes, P. Battaglino, B. J. Bloom, K. Cassella, R. Coxe, N. Crisosto, J. P. King, S. S. Kondov, K. Kotru, S. C. Larsen, J. Lauigan, B. J. Lester, M. McDonald, E. Megidish, S. Narayanaswami, C. Nishiguchi, R. Notermans, L. S. Peng, A. Ryou, T.-Y. Wu, and M. Yarwood, Assembly and coherent control of a register of nuclear spin qubits, *Nat. Commun.* **13**, 2779 (2022).
 - [24] J. K. Krondorfer and A. W. Hauser, Nuclear electric resonance for spatially resolved spin control via pulsed optical excitation in the UV-visible spectrum, *Phys. Rev. A* **108**, 053110 (2023).
 - [25] J. K. Krondorfer, M. Diez, and A. W. Hauser, Optical nuclear electric resonance in LiNa: selective addressing of nuclear spins through pulsed lasers, *Phys. Scr.* **99**, 075307 (2024).
 - [26] J. K. Krondorfer, S. Pucher, M. Diez, S. Blatt, and A. W. Hauser, Optical nuclear electric resonance as single qubit gate for trapped neutral atoms (2025), arXiv:2501.11163 [quant-ph].
 - [27] N. Stone, Table of nuclear magnetic dipole and electric quadrupole moments, *Atomic Data and Nuclear Data Tables* **90**, 75 (2005).
 - [28] G. Zu Putlitz, Bestimmung des elektrischen Kernquadrupolmomentes des ungeraden stabilen Strontium-87-Kerns, *Zeitschrift für Physik* **175**, 543 (1963).
 - [29] A. Heinz, A. J. Park, N. Šantić, J. Trautmann, S. G. Porsev, M. S. Safronova, I. Bloch, and S. Blatt, State-dependent optical lattices for the strontium optical qubit, *Phys. Rev. Lett.* **124**, 203201 (2020).
 - [30] J. Johansson, P. Nation, and F. Nori, QuTiP 2: A Python framework for the dynamics of open quantum systems, *Comput. Phys. Commun.* **184**, 1234 (2013).
 - [31] J. Johansson, P. Nation, and F. Nori, QuTiP: An open-source Python framework for the dynamics of open quan-

- tum systems, *Comput. Phys. Commun.* **183**, 1760 (2012).
- [32] H.-P. Breuer and F. Petruccione, *The Theory of Open Quantum Systems* (Oxford University Press, 2007).
- [33] M. Borkowski, L. Reichsöllner, P. Thekkeppatt, V. Barbé, T. van Roon, K. van Druten, and F. Schreck, Active stabilization of kilogauss magnetic fields to the ppm level for magnetoassociation on ultranarrow feshbach resonances, *Review of Scientific Instruments* **94**, 073202 (2023).

SUPPLEMENTARY INFORMATION: SINGLE QUDIT CONTROL IN ^{87}SR VIA OPTICAL NUCLEAR ELECTRIC RESONANCE

In this Supplementary Information, we provide an extended scan of the amplitude modulation T to illustrate the multiple equidistant transition peaks in Section S1. We provide scans of the amplitude modulation period for different system parameters in Section S2 and discuss resulting Rabi oscillations in more detail. Finally, details on the overall computational implementation are presented in Section S3.

S1. EXTENDED T SCAN – MULTIPLE TRANSITIONS

In this section, we show that full transitions occur for equidistantly spaced amplitude modulation periods T , for all one-level transitions. As explained in the main text, this is due to multi-photon-like transitions that obey the equation

$$\Delta E_{m_I \leftrightarrow m_I+1}^{\text{eff}} = n \frac{2\pi}{T}, \quad (\text{S9})$$

with $n \in \mathbb{N}$. The effective energy difference $\Delta E_{m_I \leftrightarrow m_I+1}^{\text{eff}}$ of the ground state hyperfine levels is state dependent, so the periodicity is different for different transitions $m_I \leftrightarrow m_I+1$. Figure S3 shows the multiple transition peaks for the parameters $B_0 = 3000$ G, a maximal electronic Rabi frequency $\Omega_{E,0}/2\pi = 30$ MHz, a polarization angle $\theta_0 = 60$ deg, and the laser frequency $\omega_{m_I \leftrightarrow m_I+1}$. We can see that the nuclear Rabi frequency approximately drops in a straight line for higher-order transition peaks.

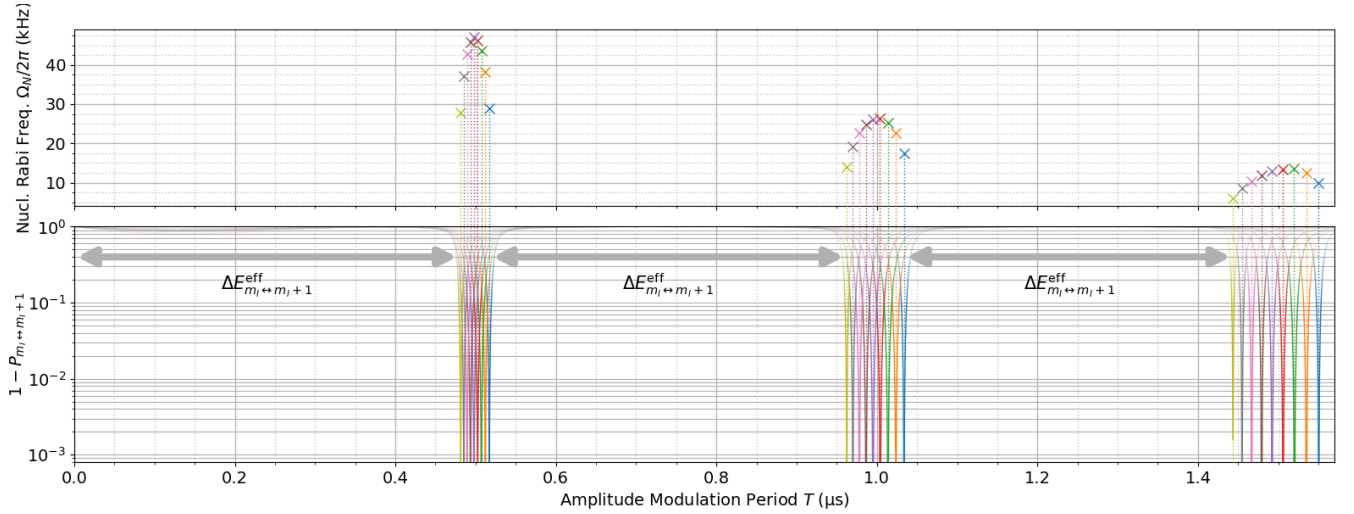


FIG. S3: Amplitude modulation period scan and corresponding nuclear Rabi frequencies. We show the π -pulse fidelity at the first flip $P_{m_I \leftrightarrow m_I+1}$ for all $\Delta m_I = \pm 1$ transitions at parameters $B_0 = 3000$ G, $\Omega_{E,0}/2\pi = 30$ MHz, $\theta_0 = 60$ deg and $\omega_{m_I \leftrightarrow m_I+1}$ as specified in the main text. Full transitions occur at different amplitude modulation periods $T_{m_I \leftrightarrow m_I+1}$ for different levels m_I . Moreover, multiple equidistantly spaced transitions occur for each level.

S2. T SCAN FOR OTHER PARAMETERS

The main text is dedicated to transitions for $B_0 = 3000$ G, a maximal electronic Rabi frequency $\Omega_{E,0}/2\pi = 30$ MHz, a polarization angle $\theta_0 = 60$ deg, and the laser frequency $\omega_{m_I \leftrightarrow m_I+1}$, respectively the detuning $\Delta_{m_I \leftrightarrow m_I+1}$, since all one-level transition can be addressed with a fidelity exceeding 99.9%. However, the ONER method is also applicable at lower magnetic fields. In these cases, not all one-level transitions may be addressed with a fidelity this high – but a subset remains usable. Therefore, it makes sense to look at scans over various system parameters for these scenarios as well. Again, we focus on one-level transitions, in contrast to Ref. 26, where two-level transitions have been considered. We investigate the system parameters $B_0 = 1000$ G, $\Omega_{E,0}/2\pi = 15$ MHz, $\theta_0 = 75$ deg, and the

corresponding $\Delta_{m_I \leftrightarrow m_I+1}$ in Figure S4. In Figure S5 we look at the transitions for system parameters $B_0 = 1500$ G, $\Omega_{E,0}/2\pi = 20$ MHz, $\theta_0 = 75$ deg, and the corresponding $\Delta_{m_I \leftrightarrow m_I+1}$.

In both cases, we obtain fidelities exceeding 99.9% for the lower four levels. For higher levels, however, the fidelity is quenched, but still exceeding 99%, as illustrated in Figures S4a and S5a. Thresholds, determined by a scan over small variations of the system parameters, are provided in Table S2 and Table S3 for each individual transition. In both cases, high fidelity transitions can still be reached for reasonable parameters and tolerance thresholds. Note that the given thresholds are estimated from below, based on the simulated transition probability with perturbed parameters. Larger perturbations might therefore still yield accurate results, especially since different parameters can be co-dependent. This is analyzed in more detail in Ref. 26.

For both parameter sets, nuclear Rabi frequencies between 10 and 25 kHz are achieved. The corresponding Rabi oscillations are illustrated in Figures S4b and S5b. The Rabi oscillations display a step-like behavior, which stems from the amplitude modulation: Each step corresponds to one cycle in the periodic modulation of the amplitude. In order to obtain smooth Rabi oscillations, the amplitude modulation frequency should be as high as possible.

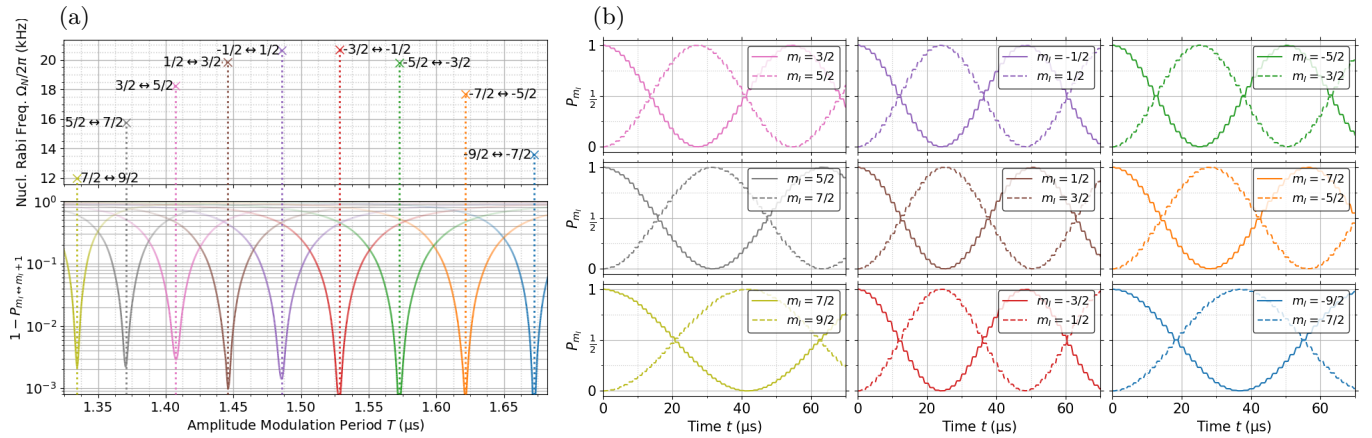


FIG. S4: (a) Amplitude modulation period scan and corresponding nuclear Rabi frequencies. We show the π -pulse fidelity at the first flip $P_{m_I \leftrightarrow m_I+1}$ for all $\Delta m_I = \pm 1$ transitions at parameters $B_0 = 1000$ G, $\Omega_{E,0}/2\pi = 15$ MHz, $\theta_0 = 75$ deg and $\omega_{m_I \leftrightarrow m_I+1}$ as specified in the main text. Full transitions occur at different amplitude modulation periods $T_{m_I \leftrightarrow m_I+1}$ for different levels m_I . (b) Rabi oscillations of all $\Delta m_I = \pm 1$ at the optimal amplitude modulation period $T_{m_I \leftrightarrow m_I+1}$.

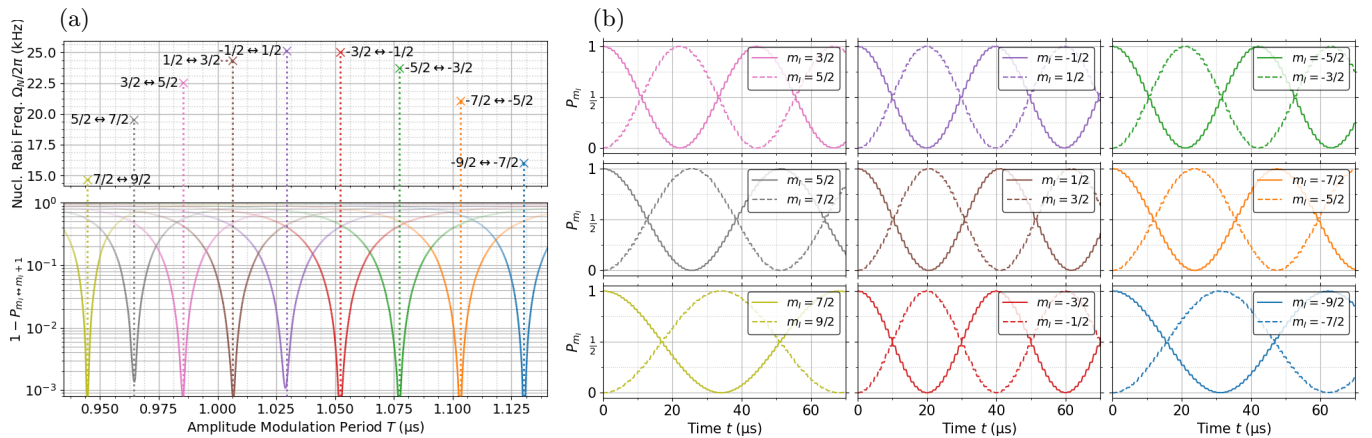


FIG. S5: (a) Amplitude modulation period scan and corresponding nuclear Rabi frequencies. We show the π -pulse fidelity at the first flip $P_{m_I \leftrightarrow m_I+1}$ for all $\Delta m_I = \pm 1$ transitions at parameters $B_0 = 1500$ G, $\Omega_{E,0}/2\pi = 20$ MHz, $\theta_0 = 75$ deg and $\omega_{m_I \leftrightarrow m_I+1}$ as specified in the main text. Full transitions occur at different amplitude modulation periods $T_{m_I \leftrightarrow m_I+1}$ for different levels m_I . (b) Rabi oscillations of all $\Delta m_I = \pm 1$ at the optimal amplitude modulation period $T_{m_I \leftrightarrow m_I+1}$.

TABLE S2: Tolerances for qudit control with ONER at $B_0 = 1000$ G, $\Omega_{E,0}/2\pi = 15$ MHz, $\theta_0 = 75$ deg, and the corresponding $\Delta_{m_I \leftrightarrow m_I+1}$ and $T_{m_I \leftrightarrow m_I+1}$. We show tolerances individually for each $\Delta m_I = \pm 1$ transition, both for 99% and 99.9% target fidelities. Deviations smaller than the listed tolerances yield spin-flip control for the corresponding transition with the respective fidelity.

Transition	$ \delta T $ (ns)		$ \delta B $ (mG)		$ \delta\Omega_E/2\pi $ (kHz)		$ \delta\theta $ (deg)		$ \delta\Delta $ (kHz)	
	99.9%	99%	99.9%	99%	99.9%	99%	99.9%	99%	99.9%	99%
$-9/2 \leftrightarrow -7/2$	0.8	3.5	380	>1000	10	35	0.15	0.7	>5000	>5000
$-7/2 \leftrightarrow -5/2$	0.8	3.5	380	>1000	10	60	0.15	0.9	>5000	>5000
$-5/2 \leftrightarrow -3/2$	0.8	4.0	400	>1000	20	60	0.15	0.9	>5000	>5000
$-3/2 \leftrightarrow -1/2$	0.8	4.0	400	>1000	15	80	0.15	1.0	>5000	>5000
$-1/2 \leftrightarrow 1/2$	-	3.8	-	>1000	-	80	-	1.0	-	>5000
$1/2 \leftrightarrow 3/2$	-	3.8	-	>1000	-	80	-	1.0	-	>5000
$3/2 \leftrightarrow 5/2$	-	3.0	-	>1000	-	80	-	1.0	-	>5000
$5/2 \leftrightarrow 7/2$	-	2.5	-	>1000	-	80	-	1.0	-	>5000
$7/2 \leftrightarrow 9/2$	-	2.0	-	>1000	-	80	-	1.0	-	>5000

TABLE S3: Tolerances for qudit control with ONER at $B_0 = 1500$ G, $\Omega_{E,0}/2\pi = 20$ MHz, $\theta_0 = 75$ deg, and the corresponding $\Delta_{m_I \leftrightarrow m_I+1}$ and $T_{m_I \leftrightarrow m_I+1}$. We show tolerances individually for each $\Delta m_I = \pm 1$ transition, both for 99% and 99.9% target fidelities. Deviations smaller than the listed tolerances yield spin-flip control for the corresponding transition with the respective fidelity.

Transition	$ \delta T $ (ns)		$ \delta B $ (mG)		$ \delta\Omega_E/2\pi $ (kHz)		$ \delta\theta $ (deg)		$ \delta\Delta $ (kHz)	
	99.9%	99%	99.9%	99%	99.9%	99%	99.9%	99%	99.9%	99%
$-9/2 \leftrightarrow -7/2$	0.5	1.8	350	>1000	8	40	0.10	0.45	>5000	>5000
$-7/2 \leftrightarrow -5/2$	0.5	2.0	450	>1000	10	50	0.10	0.60	>5000	>5000
$-5/2 \leftrightarrow -3/2$	0.5	2.0	450	>1000	15	70	0.10	0.70	>5000	>5000
$-3/2 \leftrightarrow -1/2$	0.5	2.5	450	>1000	20	70	0.15	0.80	>5000	>5000
$-1/2 \leftrightarrow 1/2$	-	2.0	-	>1000	-	70	-	0.80	-	>5000
$1/2 \leftrightarrow 3/2$	-	2.0	-	>1000	-	70	-	0.80	-	>5000
$3/2 \leftrightarrow 5/2$	-	1.8	-	>1000	-	70	-	0.80	-	>5000
$5/2 \leftrightarrow 7/2$	-	1.8	-	>1000	-	70	-	0.80	-	>5000
$7/2 \leftrightarrow 9/2$	-	1.4	-	>1000	-	70	-	0.60	-	>5000

S3. COMPUTATIONAL DETAILS

As a first step, the total time-dependent Hamiltonian is set up according to Equation (1) of the main text. As basis states we choose $|n, m_J, m_I\rangle$, with $n \in \{^1S_0, ^3P_1\}$, $m_J = 0$ for 1S_0 state and $m_J \in \{\pm 1, 0\}$ for 3P_1 state and $m_I \in \{-9/2, -7/2, \dots, 9/2\}$ as discussed in the main text. Initial states are chosen as

$$|\psi_0\rangle \in \{|^1S_0, 0, m_I\rangle \mid m_I = -9/2, \dots, 9/2\}. \quad (\text{S10})$$

Since the excited 3P_1 state decays with rate $\Gamma = 2\pi * 7.48$ kHz into the 1S_0 ground state, [23, 29] an open quantum system has to be considered with density matrix ρ . The time-evolution of the system can then be described by a Born-Markov Master equation [32] of the form

$$i\hbar\partial_t\rho = [H, \rho] + i\hbar \sum_{\alpha} k_{\alpha} \mathcal{L}[c_{\alpha}]\rho_S, \quad (\text{S11})$$

with decay strengths $k_\alpha = \Gamma$ and the Lindblad superoperator \mathcal{L} defined by

$$\mathcal{L}[c]\rho_S = c\rho_S c^\dagger - \frac{1}{2}(c^\dagger c\rho_S + \rho_S c^\dagger c) \quad (\text{S12})$$

for a collapse operator c . In our case, the collapse operators are given by

$$\begin{aligned} c_0 &= |^1S_0, 0\rangle \langle ^3P_1, 0| \otimes \mathbb{1} , \\ c_+ &= |^1S_0, 0\rangle \langle ^3P_1, +1| \otimes \mathbb{1} , \\ c_- &= |^1S_0, 0\rangle \langle ^3P_1, -1| \otimes \mathbb{1} , \end{aligned} \quad (\text{S13})$$

and model the spontaneous decay from the excited state to the ground state under the emission of a linearly, right- or left-circularly polarized photon. We simulate the time evolution given by Equation (S11) in a time interval τ with the python library QuTiP [30, 31], using the *mesolve* function. From the simulation results, we extract the occupation of the respective states.